Journal of Materials Chemistry C

PAPER

View Article Online
View Journal | View Issue

Cite this: J. Mater. Chem. C, 2017, 5, 6300

Mixed ionic–electronic conduction in $K_{1/2}Bi_{1/2}TiO_3$

Linhao Li, *[a] Ming Li, [b] Ian M. Reaney[a] and Derek C. Sinclair *[a]

Received 24th April 2017,
Accepted 1st June 2017

DOI: 10.1039/c7tc01786c

rsc.li/materials-c

Recently, it has been reported that the Pb-free piezoelectric perovskite $Na_{1/2}Bi_{1/2}TiO_3$ (NBT) can be compositionally tuned by close control of the A-site starting stoichiometry to exhibit high levels of oxide-ion conduction. The related $K_{1/2}Bi_{1/2}TiO_3$ (KBT) perovskite has also drawn considerable interest as a promising Pb-free piezoelectric material; however, its conduction properties have been less extensively investigated. Here we report on the influence of the K/Bi ratio in the starting composition on the electrical properties using a combination of impedance spectroscopy and ion-transport property measurements. KBT ceramics exhibit mixed ionic–electronic (oxide-ion) conduction with $t_{ion} \sim 0.5$ at 600–800 °C and although variations in the A-site starting stoichiometry can create a ~1 order of magnitude difference in the bulk conductivity at >500 °C, the conductivity is low (*ca.* 0.1 to 1 mS cm^{-1} at 700 °C) and the activation energy for bulk conduction remains in the range ~1.2 to 1.5 eV. The high temperature electrical transport properties of KBT are therefore much less sensitive to the starting A-site stoichiometry as compared to NBT. However, KBT ceramics exhibit non-negligible proton conduction at lower temperatures (<300 °C). For K/Bi ≥ 1 the total conductivity of KBT ceramics at room temperature can be as high as ~0.1 mS cm^{-1} under wet atmospheric conditions. This study demonstrates ionic conduction to be a common feature in $A_{1/2}Bi_{1/2}TiO_3$ perovskites, where A = Na, K.

Introduction

$(A_{1/2}Bi_{1/2})TiO_3$ perovskites (where A = Na, K) are of interest as potentially useful dielectric materials, either as Pb-free (or lower Pb-containing) piezoelectrics or as high permittivity materials for high temperature-stable ceramic capacitors.[1–8] In many cases, they are combined in solid solutions with other perovskite-based ferroelectric materials such as $PbTiO_3$ and $BaTiO_3$ to optimise the properties for these applications.[4,5,9–13]

The electrical properties of undoped $Na_{0.5}Bi_{0.5}TiO_3$ (NBT) are known to be very sensitive to the Na/Bi ratio in the starting materials and can contain high levels of oxide-ion conduction.[14,15] Three different classes of electrical behaviour can be obtained based on the magnitude of the oxide-ion transference number, t_{ion}; type I (predominantly oxide-ion conductors with $t_{ion} > 0.85$); type II (mixed oxide-ion and n-type electronic conductors with $0.6 < t_{ion} < 0.2$); and type III (dielectric, predominantly band-gap electronic conduction with $t_{ion} < 0.1$).[16] The levels of non-stoichiometry to switch between these types of behaviour is small and depends on both the nominal starting composition and the material processing routes involved in fabricating the ceramics. The presence of oxide-ion conduction in NBT is attributed to loss of Bi_2O_3 during processing and this creates the oxygen vacancies required for oxide-ion conduction in the perovskite lattice according to the Kroger–Vink equation,

$$2Bi_{Bi}^{\times} + 3O_O^{\times} \rightarrow 2V_{Bi}''' + 3V_O^{\bullet\bullet} + Bi_2O_3$$

Appropriate donor (*e.g.* Nb^{5+} for Ti^{4+}) and acceptor (*e.g.* Mg^{2+} for Ti^{4+} or Sr^{2+} for Bi^{3+}) doping can then be employed to either decrease or increase the level of oxygen vacancies and therefore fine-tune t_{ion} from low to high values in NBT to optimise compositions for potential dielectric (type III), mixed conducting (type II) or solid electrolyte (type I) applications.[14,16–19]

At present, the oxide-ion conduction mechanism in NBT remains unknown but is presumably linked to the Bi–O bonding. This, in part, is due to the complex crystal structure and polymorphism associated with NBT. NBT was initially proposed to exhibit a rhombohedral (space group *R3c*) structure with $a^-a^-a^-$ anti-phase octahedral tilting (tilt angle ~8.24°) at room temperature based on neutron powder diffraction studies.[20] Subsequent high resolution XRD data led to the suggestion that the average structure of NBT should be described more properly by a monoclinic structure (space group *Cc*).[21] Furthermore, the local structure of NBT can deviate from the average structure and lower the matrix symmetry. This can occur either by an inhomogeneous distribution of nanometre-scale platelets with a few unit cells thick of a tetragonal phase with an $a^0a^0c^+$ tilt system

[a] Department of Materials Science & Engineering, University of Sheffield, Sir Robert Hadfield Building, Mappin Street, Sheffield, S1 3JD, UK. E-mail: linhao.li@sheffield.ac.uk, d.c.sinclair@sheffield.ac.uk
[b] Department of Mechanical, Materials and Manufacturing Engineering, University of Nottingham, University Park, Nottingham, NG7 2RD, UK

or *via* a single-phase "continuous tilting" model where the in-phase ($a^-a^-c^+$) tilting only persists over a few unit cells and is superimposed on an out-of-phase ($a^-a^-a^-$) tilting matrix.[22,23] Hybridisation of the bismuth $6s^2$ lone pair electrons and the oxygen 2p orbitals leads to off-centring of Bi ions and a reduction in the coordination number which results in longer and therefore weaker Bi–O bonds.[24]

The anion conduction pathway in perovskites occurs *via* the so-called saddle point which is the space between a triangular co-ordination of two A-site cations and one B-site cation. The Na and Bi ions are disordered on the A-sites of NBT, however, recent attempts using atomistic simulations have suggested the most favourable configuration for oxide-ion migration is *via* Bi–Ti–Bi saddle points and the least favourable is *via* Na–Ti–Na saddle points.[25] The presence of Bi on the A-sites and the similar ionic radii of Bi and Na are therefore important aspects of the conduction mechanism in NBT. It is therefore interesting to investigate related perovskite materials such as $K_{0.5}Bi_{0.5}TiO_3$ (KBT) that also contain Bi on the A-site but have ions of a different size and exhibit different polymorphism (non-tilted) to NBT to improve our understanding of the structure–composition–property relationships in this class of materials.

Here we report the influence of the K/Bi starting ratio on the electrical properties of KBT and show that irrespective of the starting ratio a bulk conductivity and t_{ion} similar to type II NBT is always observed, indicating significant levels of oxide-ion conduction occurs in both NBT and KBT. In addition, KBT materials (especially those with a K-rich starting composition) are susceptible to hydration and this can result in significant levels of volumetric proton conduction below ~300 °C.

Experimental section

KBT ceramics with general formulae $K_{0.5}Bi_{0.5+x}TiO_{3+3x/2}$ ($-0.01 \leq x \leq 0.01$) and $K_{0.5+y}Bi_{0.5}TiO_{3+y/2}$ ($-0.01 \leq y \leq 0.05$) were prepared by conventional solid-state reaction. K_2CO_3 (99.5%, Sigma-Aldrich), Bi_2O_3 (99.9%, Acros Organics), and TiO_2 (99.5% purity, <100 nm particle size, Sigma-Aldrich) were used as raw materials. All reagents were dried (Bi_2O_3 and K_2CO_3 at 300 °C and TiO_2 at 900 °C) prior to batching. Appropriate amounts of raw materials were ball milled and calcined twice at 800 and 900 °C with drying and sieving afterwards. KBT pellets were sintered in air at ~1030 to 1070 °C for 2 h depending on their composition. During sintering the pellets were buried in calcined powders of the same composition. The Archimedes method was used to establish ceramic density and was in the range ~93 and 97% of the theoretical X-ray density for all samples.

The phase purity of KBT ceramics was monitored by a combination of powder X-ray diffraction (XRD) on a Stoe STADI/P transmission system and a Philips XL 30S FEG scanning electron microscope with a Noran energy dispersive X-ray analyser (SEM/EDX). Impedance spectroscopy measurements were performed on sintered ceramics coated with Au-paste electrodes using an Agilent E4980A and a Solartron Modulab. The results were corrected for sample geometry (thickness/area of pellet). To monitor moisture sensitivity of the conductivity, a wet atmosphere was generated across ceramics with electrodes in a sealed impedance rig by flowing compressed air through a bubbler which was kept in a 70 °C water bath. Impedance measurements were then made at elevated temperatures on heating and cooling.

The oxide ion transport number was measured on a ProboStat system by the electro-motive force (EMF) method at 600–800 °C. A gas concentration cell was prepared using N_2 and air to generate an oxygen partial pressure (pO_2) gradient. A YSZ tube was used as a pO_2 monitor. More detailed experimental information can be found in the ESI in ref. 13.

Mass-loss studies on KBT were performed using a PerkinElmer Pyris 1 for thermogravimetric analysis (TGA) connected to a Hiden Analytical HPR20 mass spectrometer to monitor any gas species evolved (mass spectrometry, MS) during two consecutive heating and cooling cycles.

Results

Room temperature XRD patterns of crushed pellets for both *x*- and *y*-series samples are shown in Fig. 1. All observed reflections are consistent with the reported tetragonal structure (space group *P4mm*) of KBT at room temperature with no additional reflections; calculated lattice parameters for both series are shown in Fig. 2. A-Site non-stoichiometry in the starting composition has no significant influence on the *a* axis and only a modest influence on the *c* axis. In contrast, SEM and EDS reveal a secondary phase in all KBT ceramics which is identified as $K_2Ti_6O_{13}$ based on EDX data, Fig. 3 and Table 1. The low level of Bi detected in the secondary phase analysis is attributed to the spot size used for EDX analysis which was generally comparable to or slightly larger than the size of the secondary phase being analysed and therefore includes a contribution from the matrix phase (KBT). The absence of any reflections associated with $K_2Ti_6O_{13}$ in the XRD patterns is attributed to the low volume fraction of this phase compared with the KBT matrix as revealed by SEM analysis. Significant and/or systematic variations in A-site non-stoichiometry for the *x*- and *y*-series samples was not distinguished by EDX analysis

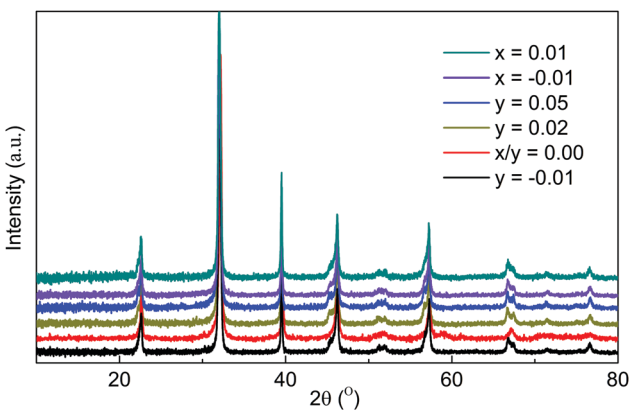

Fig. 1 Room temperature X-ray powder diffraction data of $K_{0.5}Bi_{0.5+x}TiO_{3+3x/2}$ and $K_{0.5+y}Bi_{0.5}TiO_{3+y/2}$ crushed ceramics.

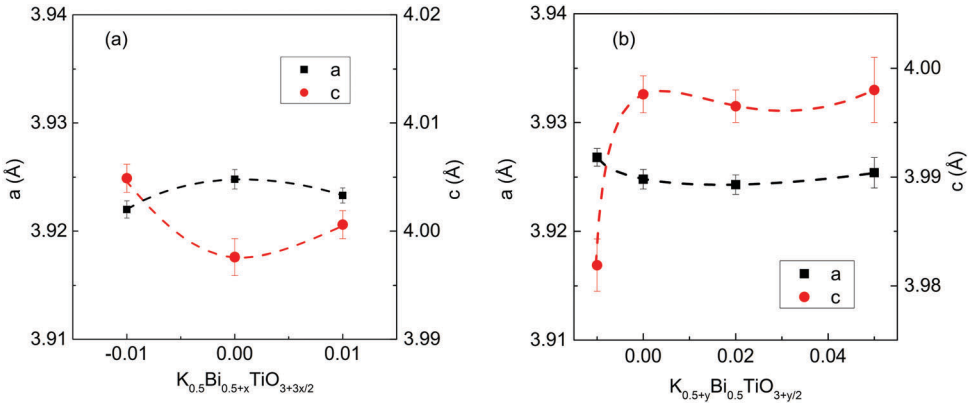

Fig. 2 Lattice parameters for (a) $K_{0.5}Bi_{0.5+x}TiO_{3+3x/2}$ and (b) $K_{0.5+y}Bi_{0.5}TiO_{3+y/2}$ crushed ceramics.

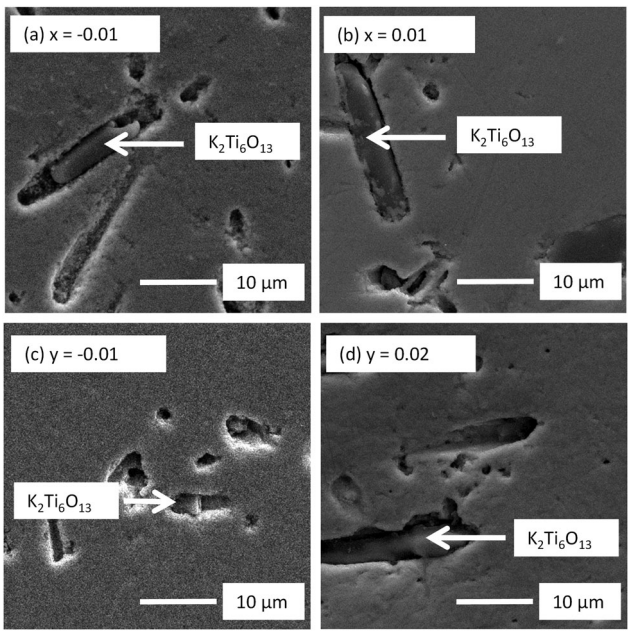

Fig. 3 SEM secondary electron images of selected (a and b) $K_{0.5}Bi_{0.5+x}TiO_{3+3x/2}$ and (c and d) $K_{0.5+y}Bi_{0.5}TiO_{3+y/2}$ ceramics highlighting the presence of $K_2Ti_6O_{13}$ as a secondary phase. Samples were polished without thermal etching.

Table 1 Chemical composition (relative cation at%) and associated error (standard deviation) by SEM/EDX of the main and secondary phases present in $K_{0.5}Bi_{0.5+x}TiO_{3+3x/2}$ and $K_{0.5+y}Bi_{0.5}TiO_{3+y/2}$ ceramics. Each value is obtained from an average of 10 analysed points. Some totals deviate from 100.0% due to rounding errors

Composition		Bi (at%)	Ti (at%)	K (at%)
$x = -0.01$	Main phase	26.6 (±0.3)	48.4 (±1.2)	25.0 (±1.1)
	$K_2Ti_6O_{13}$	1.9 (±0.5)	73.0 (±0.5)	25.1 (±0.2)
$x/y = 0.00$	Main phase	26.2 (±0.4)	48.4 (±1.4)	25.3 (±1.5)
	$K_2Ti_6O_{13}$	1.5 (±0.6)	73.9 (±0.9)	24.6 (±0.9)
$x = 0.01$	Main phase	26.9 (±0.4)	47.4 (±0.8)	25.7 (±0.6)
	$K_2Ti_6O_{13}$	1.4 (±0.8)	74.2 (±0.7)	24.4 (±1.2)
$y = -0.01$	Main phase	26.3 (±0.3)	48.6 (±0.9)	25.1 (±0.5)
	$K_2Ti_6O_{13}$	1.4 (±0.5)	73.6 (±0.4)	25.0 (±0.2)
$y = 0.02$	Main phase	26.4 (±0.2)	47.6 (±0.2)	26.0 (±0.2)
	$K_2Ti_6O_{13}$	3 (±2)	71 (±4)	26 (±2)
$K_{0.5}Bi_{0.5}TiO_3$	Expected	25.0	50.0	25.0
$K_2Ti_6O_{13}$	Expected	0.0	75.0	25.0

and all main phase KBT data were similar within instrumental errors. The average grain size of the KBT ceramics is 200–300 nm and is not significantly influenced by the starting A-site stoichiometry, Fig. 4.

Impedance complex plane, Z^*, plots for the x- and y-series of ceramics at 650 °C are shown in Fig. 5. Data for all samples consist of a single, large arc with the presence of a small, low frequency (<10 Hz) electrode-type response. To a first approximation, the large arc could be modelled with a single parallel resistor–capacitor (RC) element with an associated capacitance value consistent with a bulk paraelectric (grain) response, *e.g.* $\sim 10^{-10}$ F cm^{-1}, (C_b). The associated capacitance for the low frequency spike was in the range 10^{-3} to 10^{-5} F cm^{-1} and is consistent with typical Warburg-type diffusion. Among all samples, x and y = 0.00 possess the highest bulk resistivity (R_b) and any starting Bi non-stoichiometry (*i.e.* $\pm x$) and K-deficiency ($y < 0$) have limited influence on R_b. In contrast, increasing the starting K-content in the y-series leads to a decrease in R_b from $\sim$60 kΩ cm for y = 0.00 to $\sim$2.4 kΩ cm for y = 0.05, Fig. 5(b).

An Arrhenius plot of the temperature dependence of the bulk conductivity, σ_b, (where $\sigma_b = 1/R_b$ with R_b obtained from the intercept of the Z' axis in the Z^* plots) shows it to increase significantly with increasing K-content in the starting material whereas the activation energy for the bulk conduction, E_a, remains similar for all KBT ceramics, Fig. 6. In general, the magnitude of σ_b for the KBT series is consistent with type II (mixed conductor) and III (electronic insulator) NBTs and are much lower than type I (oxide ion conductor) NBT[14–16] as shown in Fig. 6. It is important to note that σ_b values were extracted on a cooling cycle in air from a starting temperature of $\sim$800 °C.

Prior to creating an oxygen concentration gradient for the emf measurements a small positive voltage (the voltage in emf measurement is defined as positive/negative as the electrode of

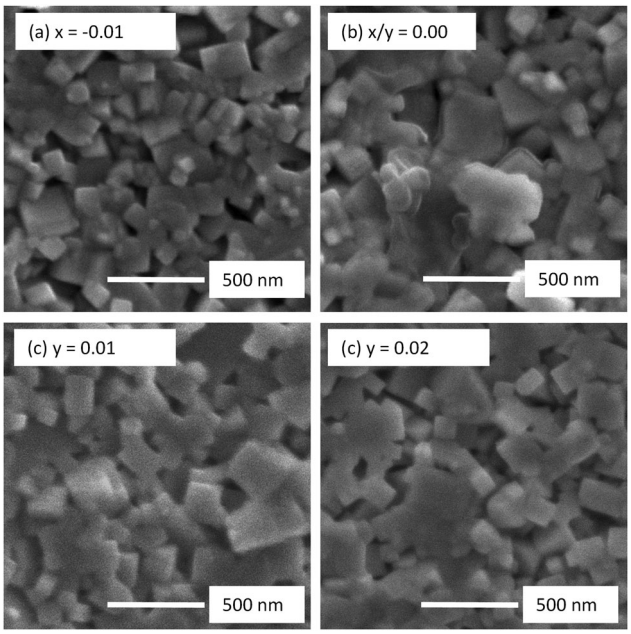

Fig. 4 SEM secondary electron images of unpolished surfaces of selected (a and b) $K_{0.5}Bi_{0.5+x}TiO_{3+3x/2}$ and (c and d) $K_{0.5+y}Bi_{0.5}TiO_{3+y/2}$ ceramics.

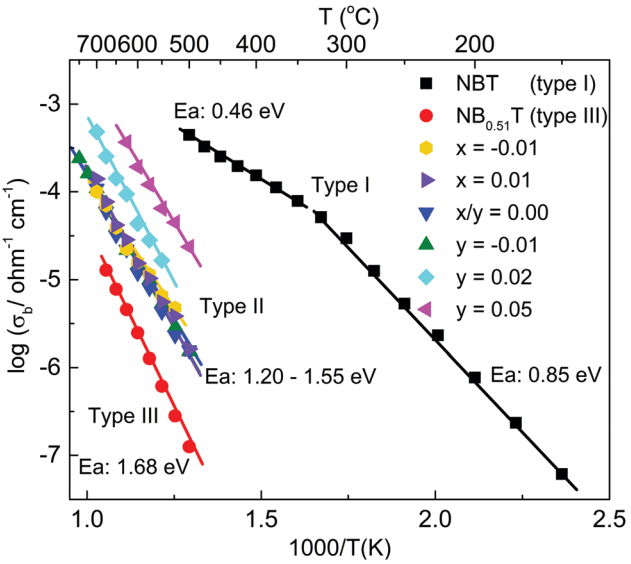

Fig. 6 Arrhenius-type plots of bulk conductivity for all $K_{0.5}Bi_{0.5+x}TiO_{3+3x/2}$ and $K_{0.5+y}Bi_{0.5}TiO_{3+y/2}$ ceramics. Conducting $Na_{0.5}Bi_{0.5}TiO_3$ (NBT) and insulating $Na_{0.5}Bi_{0.51}TiO_3$ ($NB_{0.51}T$) samples are included for reference.

gas II, inner electrode, is positive/negative, respectively Fig. 7 and Table 2) was observed when the KBT ceramics (at 600 to 800 °C) were exposed to laboratory air at the outer (gas I) electrode and to dry air at the inner electrode (gas II), Fig. 7(a). Given the absence of a pO_2 gradient, this indicated evidence of possible proton conduction in KBT ceramics. Ion transport number measurements using air and nitrogen gas to create a pO_2 gradient were performed in the range 600 to 800 °C and Table 2 highlights the importance of using dry gases to minimise the influence of water on t_{ion} for oxide-ions. Dry N_2 and lab air resulted in small negative voltages; whereas, dry N_2 and dry air resulted in significantly larger negative voltages, indicating t_{ion} with values typically ~0.5, Fig. 7(b–d) and Table 2.

In an attempt to confirm proton conduction, impedance measurements were recorded on selected KBT ceramics in a wet (high pH_2O) air atmosphere (after 16 hours exposure at room temperature, RT) and compared to those obtained in a dry air atmosphere. Z^* plots for y = 0.00 and 0.05 at RT under wet/dry flowing air are shown in Fig. 8. In both samples, the impedance in dry air (red symbols) was too large to measure at RT ($\gg$10 MΩ cm) as indicated by the near vertical response of the higher frequency Z^* data (red symbols). This confirms the arc associated with the bulk response at elevated temperatures in Z^* plots (see Fig. 5) can't be observed at RT. In contrast, the Z^* response of samples in wet flowing air at RT display a non-ideal high frequency semicircular arc (R_T ~ 250 kΩ cm for y = 0.00 and ~3 kΩ cm for y = 0.05) and a low frequency spike separated by poorly resolved features at intermediate frequencies, Fig. 8. The extracted capacitances associated with the high frequency semicircle and low frequency spike are ~5×10^{-11} and 1×10^{-6} F cm^{-1}, respectively. The low frequency spike in the Z^* plots is clearly indicative of ionic (presumably protonic)

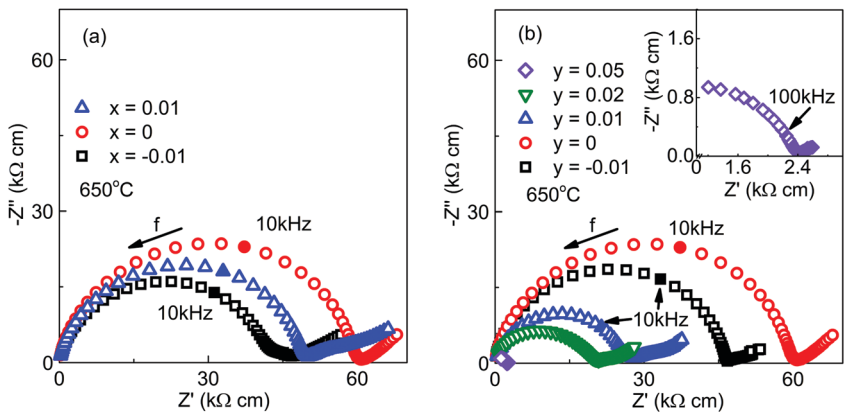

Fig. 5 Z^* plots for (a) $K_{0.5}Bi_{0.5+x}TiO_{3+3x/2}$ and (b) $K_{0.5+y}Bi_{0.5}TiO_{3+y/2}$ ceramics. Inset in (b) shows data for y = 0.05 on an expanded scale. All data were obtained in air at 650 °C and the lowest frequency was 0.1 Hz.

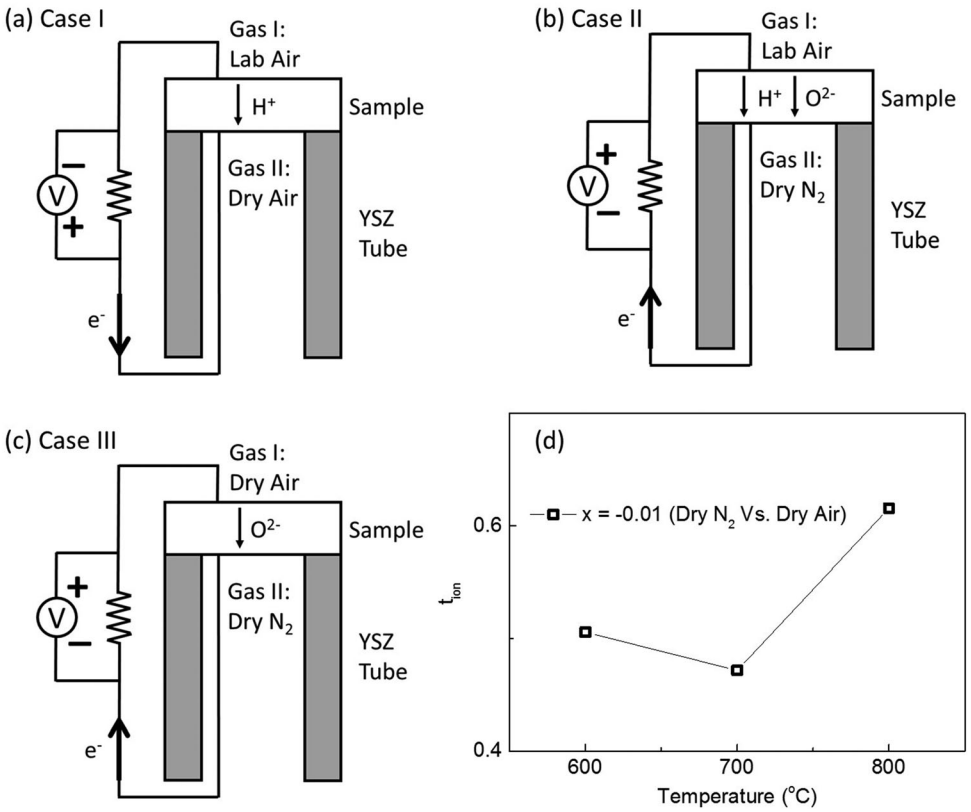

Fig. 7 (a–c) Schematic illustrations of oxygen concentration cells under various gas I and gas II conditions; (d) t_{ion} *versus* temperature for $K_{0.5}Bi_{0.49}TiO_{2.985}$ ($x = -0.01$) from EMF measurements using dry air/dry nitrogen gas (case III).

Table 2 EMF values *versus* temperature for $K_{0.5}Bi_{0.49}TiO_{2.985}$ ($x = -0.01$) oxygen concentration cells with various gases

Gas	EMF[c] (mV)					
	$x = -0.01$			YSZ		
Gas I/gas II[a]	600	700	800	600	700	800
Lab air/dry air[b]	+22.4	+18.5	+10.9	0.0	0.0	0.0
Lab air/dry N_2	−7.0	−8.3	−19.3	−95.9	−106.5	−118.5
Dry air/dry N_2	−50.2	−53.1	−76.2	−99.2	−112.7	−123.8

[a] Gas II is inside the YSZ tube whereas gas I is outside the tube. [b] Dry gas is dried with silica gel. [c] Positive/negative sign shows that the electrode of gas II is positive/negative, respectively.

conduction in these ceramics. Based on this data, it is not clear if the proton conduction observed is *via* surface, grain boundary or bulk pathways.

The total conductivity (σ_T) of KBT ceramics under a wet atmosphere based on the arc observed in Z^* plots such as Fig. 8 at RT, where $\sigma_T = 1/R_T$, are summarised in an Arrhenius plot (dashed trend lines) in Fig. 9. Also shown, are the bulk conductivity data (σ_b) of KBT ceramics measured on a cooling cycle from ~800 °C in a dry atmosphere based on the arc observed in Z^* plots at elevated temperature, *e.g.* ~650 °C, Fig. 5, where $\sigma_b = 1/R_b$, (solid trendlines) in the Arrhenius plot in Fig. 9. For comparison, data for a stoichiometric NBT type I ceramic measured under similar wet and dry atmospheres are included in Fig. 9. In the case of wet atmospheres, σ_T is highest at RT for all three samples and decreases in the order $y = 0.05$, $y = 0.00$ then stoichiometric NBT (type I). On heating up to ~300 °C, KBT ceramics show a dramatic decrease in σ_T by at least two orders of magnitude before increasing to approach values obtained for σ_b from measurements performed at elevated temperatures (*e.g.* ~500–700 °C) in dry atmospheres, Fig. 9. It is worth noting that both σ_T and σ_b are significantly higher for $y = 0.05$ compared to $y = 0.00$ for the measured temperature range. In contrast, stoichiometric NBT (type I) shows only a modest wet/dry atmosphere effect where σ_T exceeds σ_b below ~150 °C.

To establish if surface conduction occurs in KBT ceramics, a $y = 0.05$ pellet with a ring electrode on one pellet face and a complete electrode on the other face was measured (inset of Fig. 10(b)). The ring electrode was to expose a pellet face to moisture and the lateral pellet surfaces were covered with a water-resistant Si grease to minimise any lateral conduction between the electrodes *via* moisture. Given the different electrode areas it was not possible to correct the IS data with a geometric factor and values of R and C are in units of Ω and F, respectively.

Z^* plots at RT again showed a dramatic decrease in impedance with the appearance of a high frequency arc and low frequency electrode spike within a few minutes of being exposed to the wet atmosphere, Fig. 10(a). After 20 minutes exposure, the resistance associated with the high frequency arc, R_{arc} had decreased

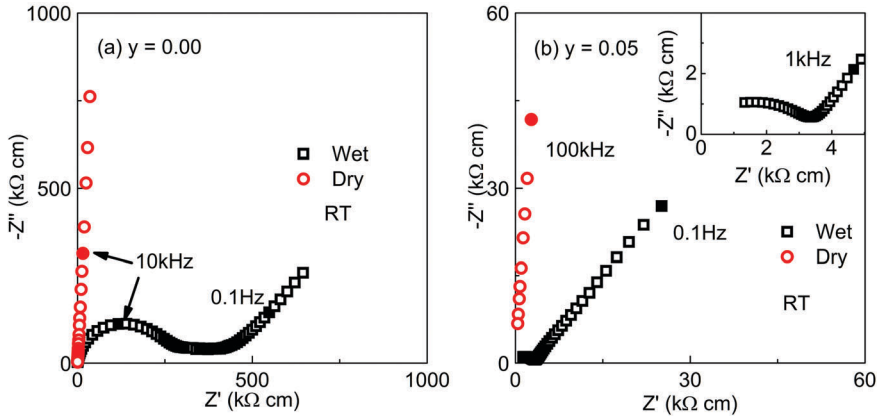

Fig. 8 Z^* plots of (a) $K_{0.5}Bi_{0.5}TiO_3$ (y = 0.00) and (b) $K_{0.55}Bi_{0.5}TiO_{3.025}$ (y = 0.05) at room temperature under wet and dry air atmospheres.

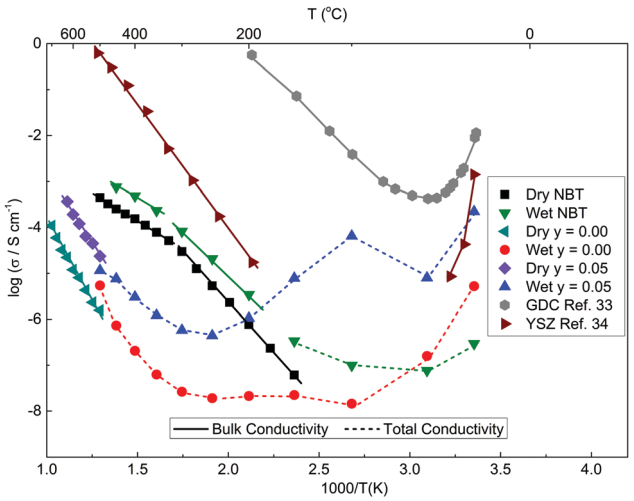

Fig. 9 Arrhenius-type plots of bulk (σ_b solid lines) and total (σ_T dashed lines) conductivity values for selected $K_{0.5+y}Bi_{0.5}TiO_{3+y/2}$ samples and stoichiometric $Na_{0.5}Bi_{0.5}TiO_3$ (NBT) measured under dry and wet atmospheres. The conductivity of the high-frequency arc of GDC[33] and YSZ[34] under wet atmosphere are included for reference.

to ~35 kΩ, see inset in Fig. 10(a). The time dependence of R_{arc} extracted from the Z^* plots is shown in Fig. 10(b) and decreases dramatically within 20 minutes of exposure. Treating the arc in Z^* plots as a single parallel RC element appears to be inappropriate based on inspection of Z'' and M'' spectroscopic plots, Fig. 10(c). Although both exhibit a single Debye-like peak, analysing the associated C values based on the relationship $\omega RC = 1$ at the peak maxima (where $\omega = 2\pi f_{max}$ where f_{max} (in Hz) is the frequency at the Debye peak maximum) give diverging values with increasing time and f_{max} values also diverge with increasing exposure time, Fig. 10(d and e), respectively. Furthermore, there is considerable broadening of the M'' peak at high frequencies after 20 min of exposure to a wet atmosphere (open red symbols, Fig. 10(c)). Finally, spectroscopic plots of C' also indicate the high frequency plateau response obtained for the bulk response (C_b) of a sample exposed to dry air is replaced by a higher capacitance frequency dependent plateau at higher frequency and is dominated by the low frequency electrode response when exposed to wet air, Fig. 10(f). These results demonstrate that protonic conduction pathways can occur within KBT ceramics, however, it is not evident whether this is dominated by a bulk, grain boundary or pore-related mechanism.

Confirmation that lateral proton conduction pathways do not dominate the conductivity below 300 °C was obtained by comparing the Z^* response of ring and full electrode samples without grease being applied to the circumference of the ceramics. These gave different values of R_T (not shown) and therefore confirmed the lateral pathway mechanism is not the dominant response.

A combination of TGA/MS measurements were performed on y = −0.01, 0.00 and 0.02 KBT crushed powders after synthesis. TGA data show a clear relationship between mass loss and K-content in the samples. K-deficient starting compositions (y = −0.01) show a modest mass loss of ~0.35% up to 600 °C on the first heating cycle that is irreversible on cooling and subsequent heating/cooling cycles, Fig. 11(a). In contrast, stoichiometric (y = 0.00) and K-excess (y = 0.02) starting compositions show corresponding mass losses of ~1.10 and 1.25%, respectively on the initial heating cycle. Although this is largely irreversible on cooling it is noteworthy that there is a small (and reversible) weight gain on cooling during the first cycle below 300 °C that can be removed on the second heating cycle but returns again on the second cooling cycle below ~300 °C, Fig. 11(a). In the case of y = 0.02 the mass loss on the first heating cycle appears to occur in three stages; a dramatic loss of ~0.6% between RT–100 °C; ~0.4% between ~100 and 300 °C; ~0.25% between 300 and 600 °C, Fig. 11(b). MS data confirmed water loss from the KBT powders as shown by the significant ion current peaks associated with water at ~130, 300 and 400 °C for y = 0.02, Fig. 11(b).

Discussion

Based on a combination of the XRD and SEM/EDX results in Fig. 1–3 and Table 1 the level of non-stoichiometry in KBT ceramics is low and all ceramics, irrespective of x and y contain

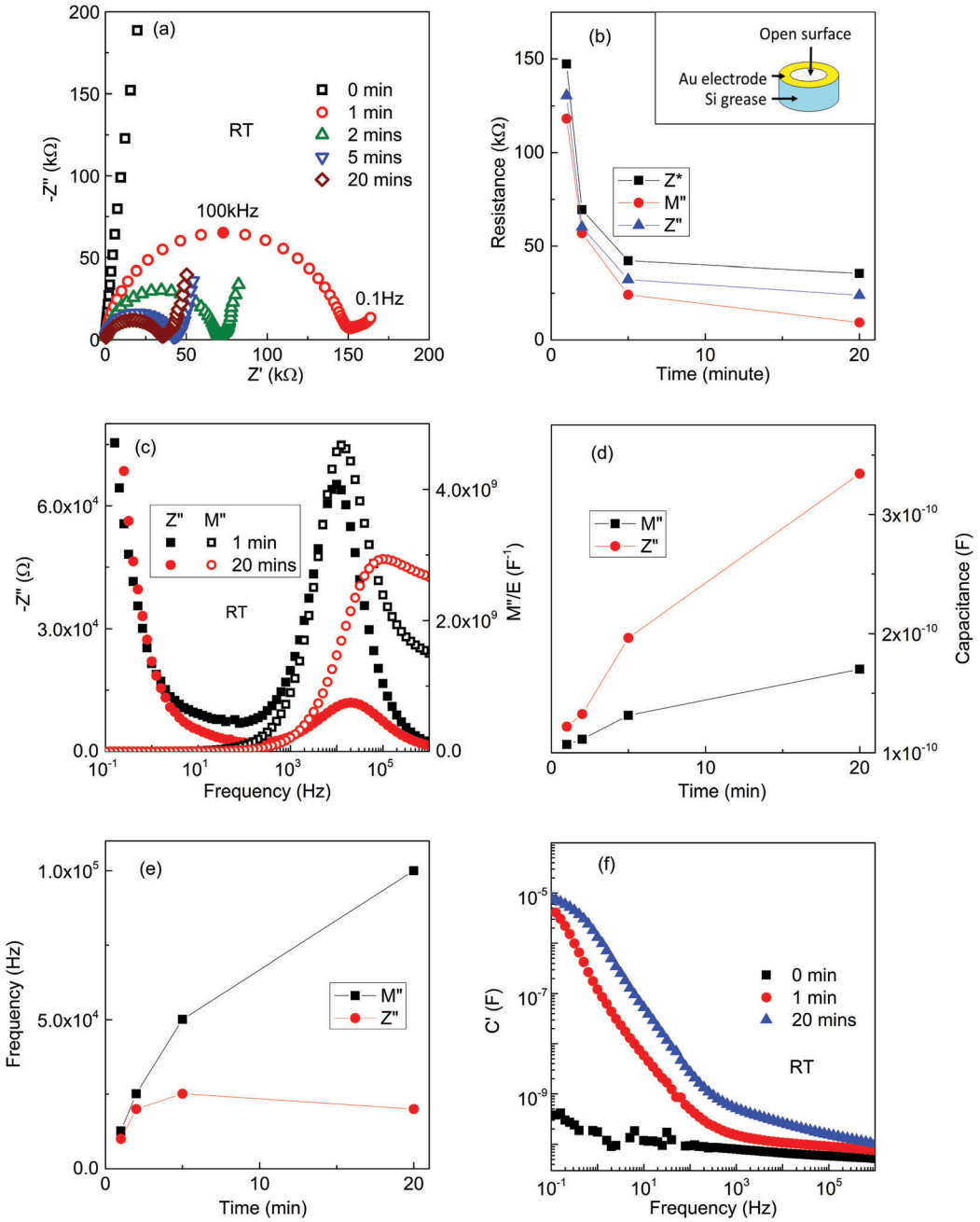

Fig. 10 (a) Z^* plots; (b) extracted R_{arc} from Z^* plots; (c) combined Z'' and M'' spectroscopic plots; (d) extracted C from Z'' and M'' spectroscopic plots; (e) f_{max} values from Z'' and M'' spectroscopic plots and (f) log C' spectroscopic plots *versus* exposure time to a wet air atmosphere at RT for a $K_{0.55}Bi_{0.5}TiO_{3.025}$ (y = 0.05) ceramic with a ring electrode and Si grease on the lateral pellet surfaces.

low levels of $K_2Ti_6O_{13}$ as a secondary phase. König *et al.* have suggested the formation of $K_2Ti_6O_{13}$ is due to thermal decomposition and evaporation of K and Bi and only forms on the outer surfaces of ceramics.[26] For KBT ceramics prepared by solid state reaction in this study, the formation of $K_2Ti_6O_{13}$ as a minor secondary phase could not be avoided. The use of sacrificial powder with the same composition being used to cover pellets during sintering and the use of nano-sized TiO_2 powder as a starting reagent to minimise sintering time are insufficient to limit volatilisation of K_2O and/or Bi_2O_3 or to suppress the formation of $K_2Ti_6O_{13}$. Although the volume fraction of $K_2Ti_6O_{13}$ is small it is not restricted to outer surfaces of ceramics and was observed on polished ceramics without thermal etching, Fig. 3.

Impedance spectroscopy results on x- and y-series ceramics measured on a cooling cycle from ~800 °C in dry air demonstrated a limited variation of *ca.* 1 order of magnitude in the bulk conductivity (σ_b) for the various samples, Fig. 5. There was no systematic trend in σ_b for the x-series; however, there is a systematic increase in σ_b with increasing K-content for

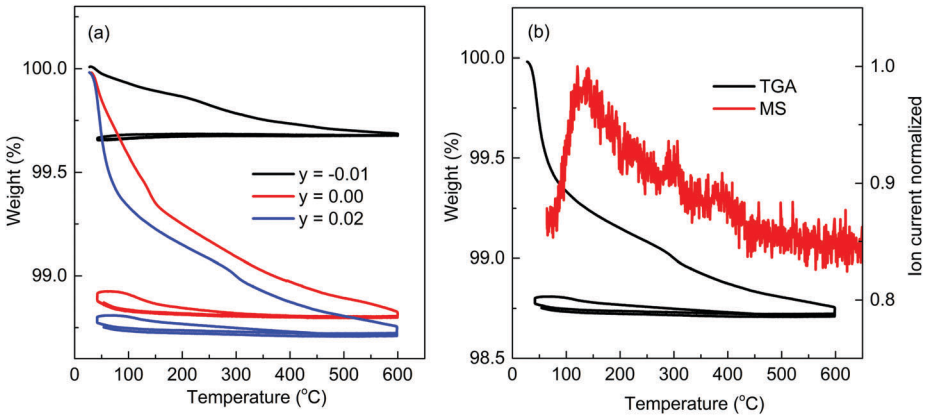

Fig. 11 (a) Heating and cooling cycle TGA data for selected $K_{0.5+y}Bi_{0.5}TiO_{3+y/2}$ crushed ceramics. (b) Mass spectroscopy data on a heating cycle of TGA experiments for $K_{0.52}Bi_{0.5}TiO_{3.01}$ (y = 0.02). TGA data are included for ease of comparison.

the y-series. The activation energy associated with σ_b was similar for all samples, ~1.2 to 1.5 eV indicating the bulk conduction mechanism is similar in all ceramics measured in a dry (lab air) atmosphere at elevated temperatures, *ca.* ~500 to 700 °C, Fig. 5. The emf measurements in the range ~600 to 800 °C using dry N_2 and dry air to create a pO_2 gradient give oxide-ion transport numbers of ~0.5 to 0.6, Fig. 7(a) indicating that KBT ceramics are mixed ionic (oxide-ion) electronic conductors under these conditions of T and pO_2. The variation in electrical properties presented demonstrate that a low level of non-stoichiometry exists in KBT that is difficult to detect by XRD and analytical SEM/EDX.

Based on a previous classification of NBT ceramics,[16] all KBT ceramics are type-II mixed ionic–electronic conductors and the magnitude of σ_b is intermediate between NBT type-I and -III as shown in Fig. 5. The presence of oxide-ion conduction and therefore oxygen deficiency in KBT is attributed to loss of Bi_2O_3 and/or K_2O during ceramic processing. The most obvious difference between KBT and NBT ceramics prepared by solid state reaction is the lack of type-I, high level oxide ion conduction in KBT ceramics. Although both are A-site Bi and Alkaline metal containing perovskites they do exhibit distinct differences and possible explanations for the absence of type-I behaviour in KBT are discussed below.

Firstly, despite the chemical similarity between K^+ and Na^+ ions, the difference in their ionic radius results in significantly different polymorphic structures leading to differences in the local Bi–O bonding and O–O separation distances that are considered to play a crucial role in the oxide-ion conduction mechanism.[14,18,19,25,27,28] Due to the larger ionic radius of K^+, there is no TiO_6 octahedral tilting and the Bi^{3+} ions are not off-centred and therefore lead to equal Bi–O bond lengths.[29] KBT exhibits the same low temperature sequence of polymorphism as ferroelectric $BaTiO_3$, *i.e.* ground state rhombohedral followed by transitions to orthorhombic, tetragonal and cubic-type structures with increasing temperature. In contrast, the smaller ionic radius of Na^+ results in TiO_6 octahedral tilting below *ca.* 520 °C with Bi^{3+} ions in off-centred and underbonded coordination environments that lead to weak Bi–O bonds. NBT exhibits complex polymorphism and various tilt structures.[21–23] Levin and Reaney[23] have suggested a 'continuous tilt' model to explain the difference in polytypes reported for NBT based on techniques used to probe the local and average structure. The influence of the larger K^+ ions on the crystal structure of KBT leads to larger O–O separation distances and more regular Bi–O bonding environments and both of these factors are likely to be detrimental to the mobility of oxide-ions and may be (at least partially) the reason for the lower level of t_{ion} and the absence of type-I behaviour in KBT ceramics.

Secondly, the existence of $K_2Ti_6O_{13}$ as a secondary phase in all the ceramics prepared in this study (albeit in low volume fractions) may have a significant influence on the composition of the KBT main phase. Given the sensitivity of the oxide-ion conduction to small variations in A- and O-site non-stoichiometry in NBT this may also be a contributing factor to the absence of type-I behaviour in our KBT ceramics. It has been shown previously[14–16] that starting compositions with Na/Bi $\geq$ 1 are type-I conductors and those with Na/Bi $<$ 1 are either type-II or -III depending on the level of excess Bi_2O_3 in the starting composition. A small excess of starting Bi_2O_3, *e.g.* $Na_{0.50}Bi_{0.51}TiO_{3.015}$ is sufficient to compensate for Bi_2O_3-loss during processing and gives rise to type-III behaviour; however, larger excesses of starting Bi_2O_3, *e.g.* $Na_{0.50}Bi_{0.55}TiO_{3.075}$ result in appreciable levels of Bi-rich secondary phase that deplete the Bi-content in the NBT phase so as to give rise to type-II behaviour.[16] The presence of $K_2Ti_6O_{13}$ as a secondary phase in all the KBT ceramics prepared in this study may deplete K from the KBT main phase resulting in K/Bi $<$ 1 and therefore favour type-II as opposed to type-I behaviour. It would be informative to prepare KBT powders by softer chemical routes such as sol–gel or hydrothermal processing where mixing is on the atomic scale to see if finer control of the stoichiometry could lead to single phase KBT ceramics free from this secondary phase and therefore give rise to KBT ceramics with higher t_{ion} and oxide-ion conductivity than that observed here.

A combination of experimental results based on impedance spectroscopy, EMF measurements using wet gases, Fig. 5–10, and TGA/MS, Fig. 11, lead to the suggestion that significant

levels of hydration occurs in powders of crushed KBT ceramics and that proton conduction can occur in KBT ceramics, especially in wet air atmospheres in a temperature range of ~RT to *ca.* 300 °C. The effects are particularly pronounced in K-rich starting compositions in the *y*-series. For example, TGA/MS of crushed KBT ceramics for $y = 0.02$ show ~1.25% mass loss on heating from RT to 600 °C that can be attributed to dehydration of water, Fig. 11(b). The TGA data also reveal that *y*-excess samples start to gain mass (and therefore hydrate) as they approach RT on a cooling cycle within the thermal analyser, Fig. 11(a). This demonstrates a strong tendency for K-rich starting KBT ceramics to absorb moisture from an air atmosphere below *ca.* 300 °C.

The presence of proton conduction in many well-known oxide-ion conductors, *e.g.* gadolina-doped ceria (GDC) and yttria-stablised zirconia (YSZ) has received increasing attention over the last few years, especially in nano-structured materials. In particular, high pressure compaction or flash sintering (*e.g.* Spark Plasma Sintering) of nanopowders to produce nano-grained ceramics[30] or the fabrication of porous and dense nanocrystalline thin films have been investigated.[31] Although it is well established 'bulk' protonic conduction can occur in oxygen-deficient fluorites and perovskites *via* the following mechanism:[32]

$$H_2O + V_O^{\bullet\bullet} + O_O^{\times} \rightarrow 2OH_O^{\bullet}$$

some studies on dense nanocrystalline GDC and YSZ ceramics have shown that the predominant proton conduction mechanism near RT can be attributed to a surface pathway (lateral pellet surfaces) instead of a volumetric (grain) mechanism.[33,34] Furthermore, Gregori *et al.*[31] have studied proton conduction in dense and porous nanocrystalline GDC thin films and concluded that the proton transport below 300 °C is also not associated with bulk or grain boundary transport but is due to residual open mesoporosity. Quantitative analysis suggested that the low temperature proton conduction can arise from space charge zones on the water side of the water/oxide interface in addition bulk water adsorbed in open pores.[31]

The wet atmosphere impedance results shown in Fig. 10 rule out a dominant lateral proton conduction mechanism in our KBT ceramics; however, the source of the volumetric conduction (*i.e.* grain, grain boundary or porosity) and whether or not it is enhanced by the presence of $K_2Ti_6O_{13}$ as a secondary phase can't be established and requires further study. A clear trend is observed, however, that the conductivity below ~300 °C of KBT ceramics (and especially K-rich samples) is sensitive to wet atmospheres and that NBT ceramics show only a modest effect below ~150 °C despite the much higher level of oxide-ion conductivity in type-I NBT, Fig. 9. Three supporting reasons for this observation are proposed.

First, K is more electropositive than Na and this makes KBT a more basic oxide than NBT and therefore more likely to hydrate. Second, proton migration in oxides is known to be faster in lattices with large cations and O–O distances.[35] as the protons require the dynamics of their attached oxygen ion to break the O–H bond. The vibrations of the oxide-ion sublattice can effectively reduce the O–H···O distance which also helps with the proton migration. Therefore, large cations and longer O–O distance provide more conducive oxygen dynamics to facilitate proton migration. This may be a crucial factor for the higher proton conduction in KBT that contain a larger cation and a longer O–O distance compared to NBT. Third, for ABO_3 perovskites there is a known correlation between the hydration enthalpy and the absolute value of the difference in electronegativity between the two cations ($\Delta X_{|A-B|}$).[35,36] The correlation is empirical and shows the hydration enthalpy becomes more negative (favourable) with decreasing $\Delta X_{|A-B|}$. This difference is 0.4 for NBT and 0.29 for KBT which means protons are more stable in KBT than in NBT and this is consistent with the larger negative temperature coefficient of the total conductivity for KBT below 300 °C. In previous studies, relatively low activation energy values compared to this study have been reported for KBT ceramics with a changing point at ~450 °C.[37,38] This phenomenon may be associated with the high proton conduction at lower temperatures and its subsequent removal by ~450 °C. The presence of protonic conduction in KBT is undesirable for dielectric/piezoelectric applications operating in the temperature range between ~25 and 300 °C and the present work indicates that K-excess starting compositions should be avoided for such applications.

Conclusions

KBT is a mixed oxide-ion electronic conductor at high temperatures (>600 °C). The level of mixed conductivity in this temperature range is relatively insensitive to the A-site starting stoichiometry and in contrast to NBT, high levels of oxide-ion conduction (solid electrolyte behaviour) can't be induced in undoped KBT ceramics prepared under the processing conditions employed in this study. The lack of high levels of oxide-ion conduction may be linked to the difference in polymorphic perovskite structures of NBT and KBT. Volumetric proton conduction pathways occur in KBT ceramics below ~300 °C when they have been exposed to wet atmospheres near room temperature. Although the conduction mechanism remains unknown, the K content in the starting composition plays a crucial role with higher K contents leading to higher proton conduction. As a consequence, K-rich starting compositions should be avoided when producing KBT-based dielectric/piezoelectric devices where leakage conductivity is to be minimised.

Acknowledgements

We thank the EPSRC for funding (A new family of electrolytes based on $Na_{1/2}Bi_{1/2}TiO_3$ for intermediate-temperature solid oxide fuel cells (EP/L027348/1) and Sustainability and Substitution of Functional Materials and Devices (EP/L017563/1)); Mr Christopher Tumilson (Queens University, Belfast) and Prof. Chris Hardacre (University of Manchester) for performing Thermogravimetric and Mass Spectrometry Analysis.

References

1 Y. Hiruma, H. Nagata and T. Takenaka, Thermal Depoling Process and Piezoelectric Properties of Bismuth Sodium Titanate Ceramics, *J. Appl. Phys.*, 2009, **105**(8), 84112.

2 Y. S. Sung, J. M. Kim, J. H. Cho, T. K. Song, M. H. Kim and T. G. Park, Effects of Bi Nonstoichiometry in $(Bi_{0.5+x}Na_{0.5})TiO_3$ Ceramics, *Appl. Phys. Lett.*, 2011, **98**(1), 12902.

3 R. Dittmer, E. Aulbach, W. Jo, K. G. Webber and J. Rödel, Large Blocking Force in $Bi_{1/2}Na_{1/2}TiO_3$-Based Lead-Free Piezoceramics, *Scr. Mater.*, 2012, **67**(1), 100–103.

4 T. Takenaka, K. Maruyama and K. Sakata, $(Bi_{1/2}Na_{1/2})TiO_3$-$BaTiO_3$ System for Lead-Free Piezoelectric Ceramics, *Jpn. J. Appl. Phys.*, 1991, **30**(part 1, no. 9B), 2236–2239.

5 B. J. Chu, D. R. Chen, G. R. Li and Q. R. Yin, Electrical Properties of $Na_{1/2}Bi_{1/2}TiO_3$-$BaTiO_3$ Ceramics, *J. Eur. Ceram. Soc.*, 2002, **22**(13), 2115–2121.

6 A. Sasaki, T. Chiba, Y. Mamiya and E. Otsuki, Dielectric and Piezoelectric Properties of $(Bi_{0.5}Na_{0.5})TiO_3$–$(Bi_{0.5}K_{0.5})TiO_3$ Systems, *Jpn. J. Appl. Phys.*, 1999, **38**, 5564–5567.

7 T. Wada, K. Toyoike, Y. Imanaka and Y. Matsuo, Dielectric and Piezoelectric Properties of $(A_{0.5}Bi_{0.5})TiO_3$–$ANbO_3$ (A = Na, K) Systems, *Jpn. J. Appl. Phys.*, 2001, **40**(part 1, no. 9B), 5703–5705.

8 S. Zhao, G. Li, A. Ding, T. Wang and Q. Yin, Ferroelectric and Piezoelectric Properties of $(Na, K)_{0.5}Bi_{0.5}TiO_3$ Lead Free Ceramics, *J. Phys. D: Appl. Phys.*, 2006, **39**(10), 2277–2281.

9 Y. Hiruma, R. Aoyagi, H. Nagata and T. Takenaka, Piezoelectric Properties of $BaTiO_3$–$(Bi_{1/2}K_{1/2})TiO_3$ Ferroelectric Ceramics, *Jpn. J. Appl. Phys.*, 2004, **43**(11A), 7556–7559.

10 S. Saïd and J. P. Mercurio, Relaxor Behaviour of Low Lead and Lead Free Ferroelectric Ceramics of the $Na_{0.5}Bi_{0.5}TiO_3$–$PbTiO_3$ and $Na_{0.5}Bi_{0.5}TiO_3$–$K_{0.5}Bi_{0.5}TiO_3$ Systems, *J. Eur. Ceram. Soc.*, 2001, **21**(10–11), 1333–1336.

11 P. Marchet, E. Boucher, V. Dorcet and J. P. Mercurio, Dielectric Properties of Some Low-Lead or Lead-Free Perovskite-Derived Materials: $Na_{0.5}Bi_{0.5}TiO_3$–$PbZrO_3$, $Na_{0.5}Bi_{0.5}TiO_3$–$BiScO_3$ and $Na_{0.5}Bi_{0.5}TiO_3$, *J. Eur. Ceram. Soc.*, 2006, **26**(14), 3037–3041.

12 J. Rödel, W. Jo, K. T. P. Seifert, E.-M. Anton, T. Granzow and D. Damjanovic, Perspective on the Development of Lead-Free Piezoceramics, *J. Am. Ceram. Soc.*, 2009, **92**(6), 1153–1177.

13 V. A. Isupov, Ferroelectric $Na_{0.5}Bi_{0.5}TiO_3$ and $K_{0.5}Bi_{0.5}TiO_3$ Perovskites and Their Solid Solutions, *Ferroelectrics*, 2005, **315**(1), 123–147.

14 M. Li, M. J. Pietrowski, R. A. De Souza, H. Zhang, I. M. Reaney, S. N. Cook, J. A. Kilner and D. C. Sinclair, A Family of Oxide Ion Conductors Based on the Ferroelectric Perovskite $Na_{0.5}Bi_{0.5}TiO_3$, *Nat. Mater.*, 2014, **13**(1), 31–35.

15 M. Li, H. Zhang, S. N. Cook, L. Li, J. A. Kilner, I. M. Reaney and D. C. Sinclair, Dramatic Influence of A-Site Nonstoichiometry on the Electrical Conductivity and Conduction Mechanisms in the Perovskite Oxide $Na_{0.5}Bi_{0.5}TiO_3$, *Chem. Mater.*, 2015, **27**(2), 629–634.

16 L. Li, M. Li, H. Zhang, I. M. Reaney and D. C. Sinclair, Controlling Mixed Conductivity in $Na_{1/2}Bi_{1/2}TiO_3$ Using A-Site Non-Stoichiometry and Nb-Donor Doping, *J. Mater. Chem. C*, 2016, **4**(24), 5779–5786.

17 M. Li, L. Li, J. Zang and D. C. Sinclair, Donor-Doping and Reduced Leakage Current in Nb-Doped $Na_{0.5}Bi_{0.5}TiO_3$, *Appl. Phys. Lett.*, 2015, **106**(10), 102904.

18 F. Yang, P. Wu and D. C. Sinclair, Enhanced Bulk Conductivity of A-Site Divalent Acceptor-Doped Non-Stoichiometric Sodium Bismuth Titanate, *Solid State Ionics*, 2017, **299**, 38–45.

19 F. Yang, H. Zhang, L. Li, I. M. Reaney and D. C. Sinclair, High Ionic Conductivity with Low Degradation in A-Site Strontium-Doped Nonstoichiometric Sodium Bismuth Titanate Perovskite, *Chem. Mater.*, 2016, **28**(15), 5269–5273.

20 G. O. Jones and P. A. Thomas, Investigation of the Structure and Phase Transitions in the Novel A-Site Substituted Distorted Perovskite Compound $Na_{0.5}Bi_{0.5}TiO_3$, *Acta Crystallogr., Sect. B: Struct. Sci.*, 2002, **58**(2), 168–178.

21 E. Aksel, J. S. Forrester, B. Kowalski, J. L. Jones and P. A. Thomas, Phase Transition Sequence in Sodium Bismuth Titanate Observed Using High-Resolution X-Ray Diffraction, *Appl. Phys. Lett.*, 2011, **99**(22), 222901.

22 V. Dorcet and G. Trolliard, A Transmission Electron Microscopy Study of the A-Site Disordered Perovskite $Na_{0.5}Bi_{0.5}TiO_3$, *Acta Mater.*, 2008, **56**(8), 1753–1761.

23 I. Levin and I. M. Reaney, Nano- and Mesoscale Structure of $Na_{1/2}Bi_{1/2}TiO_3$: A TEM Perspective, *Adv. Funct. Mater.*, 2012, **22**(16), 3445–3452.

24 D. Schütz, M. Deluca, W. Krauss, A. Feteira, T. Jackson and K. Reichmann, Lone-Pair-Induced Covalency as the Cause of Temperature- and Field-Induced Instabilities in Bismuth Sodium Titanate, *Adv. Funct. Mater.*, 2012, **22**(11), 2285–2294.

25 X. He and Y. Mo, Accelerated Materials Design of $Na_{0.5}Bi_{0.5}TiO_3$ Oxygen Ionic Conductors Based on First Principles Calculations, *Phys. Chem. Chem. Phys.*, 2015, **17**, 18035–18044.

26 J. König, M. Spreitzer, B. Jančar, D. Suvorov, Z. Samardžija and A. Popovič, The Thermal Decomposition of $K_{0.5}Bi_{0.5}TiO_3$ Ceramics, *J. Eur. Ceram. Soc.*, 2009, **29**(9), 1695–1701.

27 D. S. Keeble, E. R. Barney, D. A. Keen, M. G. Tucker, J. Kreisel and P. A. Thomas, Bifurcated Polarization Rotation in Bismuth-Based Piezoelectrics, *Adv. Funct. Mater.*, 2013, **23**(2), 185–190.

28 K.-C. Meyer and K. Albe, Influence of Phase Transitions and Defect Associates on the Oxygen Migration in the Ion Conductor $Na_{1/2}Bi_{1/2}TiO_3$, *J. Mater. Chem. A*, 2017, **5**(9), 4368–4375.

29 M. Otoničar, S. D. Škapin, B. Jančar, R. Ubic and D. Suvorov, Analysis of the Phase Transition and the Domain Structure in $K_{0.5}Bi_{0.5}TiO_3$ Perovskite Ceramics by In Situ XRD and TEM, *J. Am. Ceram. Soc.*, 2010, **93**(12), 4168–4173.

30 S. Miyoshi, Y. Akao, N. Kuwata, J. Kawamura, Y. Oyama, T. Yagi and S. Yamaguchi, Low-Temperature Protonic Conduction Based on Surface Protonics: An Example of Nanostructured Yttria-Doped Zirconia, *Chem. Mater.*, 2014, **26**(18), 5194–5200.

31 G. Gregori, M. Shirpour and J. Maier, Proton Conduction in Dense and Porous Nanocrystalline Ceria Thin Films, *Adv. Funct. Mater.*, 2013, **23**(47), 5861–5867.

32 H. Iwahara, Proton Conducting Ceramics and Their Applications, *Solid State Ionics*, 1996, **86–88**(part 1), 9–15.
33 D. Pérez-Coll and G. C. Mather, Electrical Transport at Low Temperatures in Dense Nanocrystalline Gd-Doped Ceria, *Solid State Ionics*, 2010, **181**(1–2), 20–26.
34 C. Tandé, D. Pérez-Coll and G. C. Mather, Surface Proton Conductivity of Dense Nanocrystalline YSZ, *J. Mater. Chem.*, 2012, **22**(22), 11208.
35 T. Norby, M. Widerøe, R. Glöckner and Y. Larring, Hydrogen in Oxides, *Dalton Trans.*, 2004, 3012–3018.
36 T. Norby, Proton Conduction in Solids: Bulk and Interfaces, *MRS Bull.*, 2009, **34**(12), 923–928.
37 P. V. B. Rao and T. B. Sankaram, Impedance Spectroscopy Studies of $K_{0.5}Bi_{0.5}TiO_3$, *J. Electroceram.*, 2010, **25**(1), 60–69.
38 P. V. B. Rao, Electrical Properties of $K_{0.5}Bi_{0.5}TiO_3$, *J. Alloys Compd.*, 2009, **467**(1), 293–298.